

LETTER TO THE EDITOR

# Discovery of a new N-emitter in the epoch of reionization

D. Schaerer<sup>1,2</sup>, R. Marques-Chaves<sup>1</sup>, M. Xiao<sup>1</sup>, D. Korber<sup>1</sup>

<sup>1</sup> Observatoire de Genève, Université de Genève, Chemin Pegasi 51, 1290 Versoix, Switzerland

<sup>2</sup> CNRS, IRAP, 14 Avenue E. Belin, 31400 Toulouse, France

Accepted for publication in A&A Letters

## ABSTRACT

We report the discovery of a compact star-forming galaxy at  $z = 9.380$  in the GOODS-North field (named GN-z9p4) which shows numerous strong UV-optical emission lines and a single UV line, N IV]  $\lambda 1486$ . This makes GN-z9p4 the third-highest redshift N-emitter known to date. We determine the nebular abundances of H, C, N, O and Ne, size, and other physical properties of this object, and compare them to those of the other N-emitters known so far and to other star-forming galaxies. Using the direct method we find a metallicity  $12 + \log(\text{O}/\text{H}) = 7.37 \pm 0.15$ , one of the lowest among the N-emitters. The N/O abundance ratio is highly super-solar, and C/O and Ne/O normal compared to other galaxies at low metallicity. We show that the compactness of GN-z9p4 (with effective radius  $118 \pm 16$  pc at  $2 \mu\text{m}$ ) and other N-emitters translates into very high stellar mass and SFR surface densities, which could be a criterium to identify other N-emitters. Future studies and larger samples are needed to understand these recently discovered, rare, and enigmatic objects.

**Key words.** Galaxies: high-redshift – Galaxies: ISM – Cosmology: dark ages, reionization, first stars

## 1. Introduction

Among the major surprises revealed by spectroscopic observations of the distant Universe with the James Webb Space Telescope (JWST) is arguably the spectrum of the  $z = 10.6$  galaxy GN-z11. It shows a very peculiar rest-UV spectrum dominated by N IV]  $\lambda 1486$  and N III]  $\lambda 1750$  lines, which are usually not seen, and by C III]  $\lambda 1909$  (Bunker et al. 2023). Quantitative analysis of the rest-UV and optical lines of this object showed quickly that the exceptional strength of the Nitrogen lines indicate a high (super-solar) N/O abundance in an object with low metallicity ( $12 + \log(\text{O}/\text{H}) \approx 7.6 - 8.0$  Bunker et al. 2023; Cameron et al. 2023; Senchyna et al. 2024), which was essentially unseen of until then.

The peculiar abundances of GN-z11 have triggered numerous studies exploring the nucleosynthetic origin and physical processes which can explain its special abundance ratios. A similarity with Globular Cluster abundances has been noted (see Senchyna et al. 2024; Charbonnel et al. 2023), and as of now, the following sources or scenarios have been proposed to explain the observed high N/O abundance of GN-z11: Wolf-Rayet Stars, Very massive stars ( $\sim 100 - 400 M_{\odot}$ ), AGB stars, Supermassive stars (with masses  $\gtrsim 10^{3-4} M_{\odot}$  and of normal metallicity or Population III), a top-heavy IMF, Wolf-Rayet stars with intermittent star-formation, or tidal disruption events (Bunker et al. 2023; Cameron et al. 2023; Charbonnel et al. 2023; Nagele & Umeda 2023; Watanabe et al. 2024; Kobayashi & Ferrara 2024; Bekki & Tsujimoto 2023; D’Antona et al. 2023; Vink 2023; Maiolino et al. 2024; Nandal et al. 2024). No consensus has yet been reached on this question. However, the possibility that N-emitters could be signposts of Globular clusters in formation, supermassive stars, or other

“exotic” phenomena, clearly shows the interest of better understanding such objects.

After the discovery of GN-z11, several groups have searched for more objects exhibiting N IV]  $\lambda 1486$  and/or N III]  $\lambda 1750$  emission lines (hereafter referred to as N-emitters) resulting in 10 such objects, some of them previously known: Mrk 996, the Sunburst cluster, the Lynx arc, SMACS 2031, GS\_3073, RXCJ2248-4431, GLASS\_150008, CEERS-1019, GN-z11, and GHZ2/GLASS-z12 (see Senchyna et al. 2024; Pascale et al. 2023; Marques-Chaves et al. 2024; Ji et al. 2024; Topping et al. 2024; Isobe et al. 2023; Castellano et al. 2024, and references therein). These objects include the core of a peculiar low-redshift dwarf galaxy (Mrk 996), strongly lensed clusters or star-forming regions at  $z \sim 2 - 4$ , compact high-redshift galaxies from  $z \sim 6 - 12$ , and one Type 1 AGN at  $z = 5.55$ . Among this diversity, all of them share super-solar N/O abundances, the presence of gas at unusually high densities, and they are found at metallicities  $12 + \log(\text{O}/\text{H}) \sim 7.4 - 8.3$ .

Here we report the discovery of a new N-emitter at  $z = 9.4$  (named GN-z9p4), the third highest in redshift, whose rest-UV spectrum is dominated by N IV]  $\lambda 1486$ . The available JWST observations allow us to determine accurate chemical abundances of H, N, O, Ne, and an upper limit on C. The source is among the, or possibly the most-metal poor N-emitter found so far. It is also very compact, suggesting that N-emitters may be exclusively found in regions of extremely high stellar mass and SFR densities.

## 2. GN-z9p4: a new N-emitter at high redshift

GN-z9p4 ( $\alpha, \delta$  [J2000] = 189.016995, 62.241582) was identified as a  $z \sim 9.4$  galaxy by one of the authors from search-

arXiv:2406.08408v1 [astro-ph.GA] 12 Jun 2024

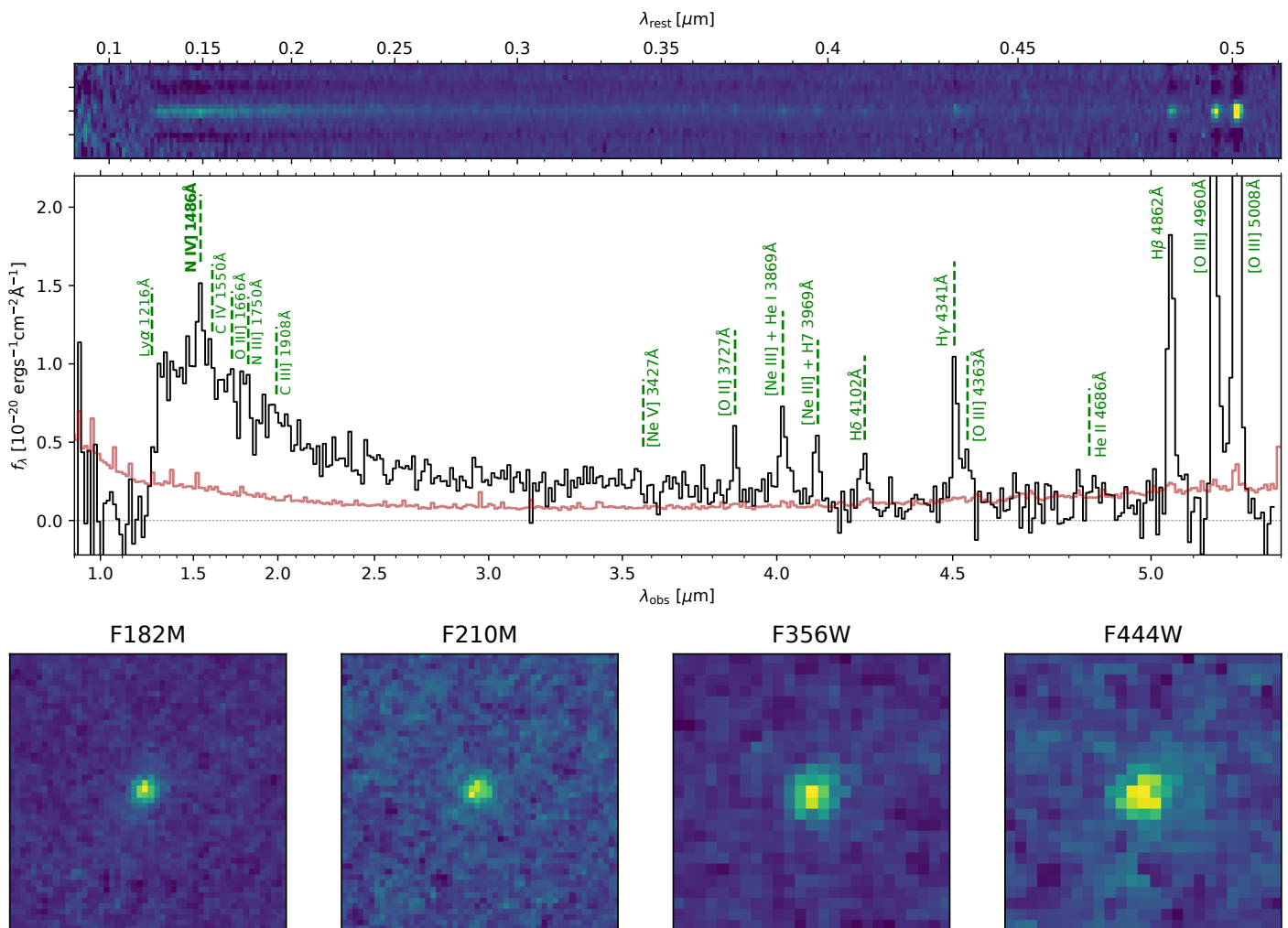


**Fig. 1.** *Top:* JWST NIRSpec/PRISM 1D and 2D spectra of GN-z9p4 at  $z = 9.38$ . The low-resolution spectrum is shown in black, and the  $1\sigma$  uncertainty in red. Vertical dashed lines (green) mark the position of detected or un-detected nebular emission lines. X-axis at the bottom and top refer to the observed and rest-frame wavelengths in  $\mu\text{m}$ , respectively. *Bottom:* Postage stamps, of total size  $1'' \times 1''$  (corresponding 4.4 kpc  $\times$  4.4 kpc physical size at  $z = 9.38$ ), of GN-z9p4 between 1.8 and 4.4  $\mu\text{m}$ .

ing the DAWN JWST Archive (DJA)<sup>1</sup> database for distant galaxies. It was identified as an LBG earlier with a photometric redshift of  $z = 9.5 \pm 0.4$  by Oesch et al. (2014). Inspection of the available JWST/NIRSpec PRISM spectrum quickly revealed a peculiar rest-UV spectrum dominated by one line, which we identified later as N IV]  $\lambda 1486$ .

### 2.1. JWST NIRSpec and NIRCcam observations

The JWST/NIRSpec spectrum of GN-z9p4 was taken by the GTO program "NIRCcam-NIRSpec galaxy assembly survey - GOODS-N" on February 7, 2023 with the low-resolution PRISM ( $R \simeq 100$ ) and coverage  $\sim 1 - 5\mu\text{m}$ . The observations consist of slitlets of 3 shutters, with the 3-point nod with an aperture position angle  $\text{PA} \simeq 19.58$  deg (see details in Eisenstein et al. 2023). The total exposure time was 6127 seconds, split into 6 individual exposures of 14 groups each. The reduced spectrum, shown in Figure 1, was obtained from the DJA database. The calibration reference data system context `jwst_1183.pmap` was used to correct spectra for flat-field and implement the wavelength

and flux calibrations. Details of the data reduction are given in Heintz et al. (2024).

GN-z9p4 was also observed with JWST/NIRCcam with the F182M, F210M, F356W, and F444W filters. These images are obtained from the DJA Imaging Data Products and were reduced using the `grizli` reduction pipeline, which includes procedures for masking the snowball artifacts and minimizing the impact of  $1/f$  noise. For the photometry we proceed as in Weibel et al. (2024). GN-z9p4 shows a very compact morphology in all NIRCcam filters, as will be quantified below.

To account for wavelength-dependent slit losses and absolute flux calibration, we derive the synthetic photometry of NIRSpec spectrum through each NIRCcam filter bandpass and compared it to that obtained from observed photometry. We find that the synthetic flux densities match well, with an average offset of  $\simeq 16\%$ , within the  $1\sigma$  uncertainties of the PRISM spectrum. No correction was thus made.

### 2.2. Emission line measurements

As shown in Figure 1, GN-z9p4 shows a blue spectrum, strong emission lines in the rest-frame optical, and a sin-

<sup>1</sup> <https://dawn-cph.github.io/dja>

**Table 1.** Emission line flux (in  $10^{-18}$  erg s $^{-1}$  cm $^{-2}$ ) and equivalent width (in Å) measurements or  $3\sigma$  upper limits for GN-z9p4.

Line	Flux	EW <sub>rest</sub>
N IV] $\lambda\lambda$ 1483, 1486	$2.913 \pm 0.53$	$31.8 \pm 6.46$
C IV $\lambda\lambda$ 1548, 1550	$< 1.56$	$< 19.1$
O III] $\lambda\lambda$ 1661, 1666	$< 1.08$	$< 14.7$
N III] $\lambda$ 1750	$< 1.32$	$< 19.7$
C III] $\lambda\lambda$ 1907, 1909	$< 1.11$	$< 18.9$
[Ne v] $\lambda$ 3427	$< 0.39$	$< 15.9$
[O II] $\lambda\lambda$ 3727, 3729	$0.683 \pm 0.20$	$38.8 \pm 13.57$
[Ne III]+He I $\lambda$ 3869	$1.374 \pm 0.24$	$84.9 \pm 24.08$
[Ne III] + H7 $\lambda$ 3968	$0.824 \pm 0.15$	$54.0 \pm 17.4$
H $\delta$ $\lambda$ 4101	$0.976 \pm 0.223$	$111.7 \pm 46.8$
H $\gamma$ $\lambda$ 4340	$1.760 \pm 0.18$	$151.0 \pm 22.0$
[O III] $\lambda$ 4363	$0.691 \pm 0.16$	$59.3 \pm 15.3$
He II $\lambda$ 4686	$< 0.54$	$< 44.7$
H $\beta$ $\lambda$ 4861	$3.314 \pm 0.14$	$284.4 \pm 34.0$
[O III] $\lambda$ 4959	$6.032 \pm 0.24$	$517.6 \pm 42.7$
[O III] $\lambda$ 5007	$16.250 \pm 0.18$	$1394.5 \pm 112.2$

gle clear emission line detection in the rest-UV. The systemic redshift of GN-z9p4 derived from the rest-optical lines (centroids of H $\beta$ , [O III]  $\lambda\lambda$ 4959,5007) is  $z_{\text{sys}} = 9.37956 \pm 0.00017$ . The rest-UV line is therefore clearly identified as N IV]  $\lambda$ 1486. Since this is the strongest rest-UV line, we classify this galaxy as a N-emitter, in analogy with the other rare objects recently discovered with the JWST (see above). After GLASS-z12 at  $z = 12.342$  and GN-z11 at  $z = 10.6$ , this detection makes GN-z9p4 the third most distant galaxy among the class of rare N-emitters, which now counts 6 objects at  $z > 6$  (see Castellano et al. 2024; Bunker et al. 2023; Marques-Chaves et al. 2024; Topping et al. 2024; Isobe et al. 2023) and 11 in total.

The rest-optical spectrum of GN-z9p4 shows H lines from the Balmer series, [O II]  $\lambda$ 3727, [O III]  $\lambda\lambda$ 4959,5007, the auroral [O III] $\lambda$ 4363, and [Ne III]  $\lambda$ 3869+He I, which have now often been seen in JWST spectra. In total, we detect 10 emission lines with a significance larger than  $3\sigma$ . To measure the line fluxes we fit simultaneously Gaussian profiles and a power-law to the continuum, as described in Marques-Chaves et al. (2024). Table 1 summarizes our flux and rest-frame equivalent width measurements, as well as upper limits for several important lines. We note that GN-z9p4 shows very strong lines, with equivalent widths exceeding largely those of the previously identified N-emitters at  $z > 8$  (CEERS-1019, GN-z11, GLASS-z12). The Balmer lines are compatible with no extinction, although with large uncertainties, allowing  $0 \leq E(B-V) \lesssim 0.2$ .

### 3. Physical properties of GN-z9p4 and other N-emitters

#### 3.1. Nature of GN-z9p4

What powers the emission lines of GN-z9p4? None of the high-ionization lines observed in AGN are detected. For He II we derive a  $3\sigma$  upper limit  $\text{He II}/\text{H}\beta \leq 0.16$ , and [Ne v]  $\lambda$ 3427 is also not detected with  $[\text{Ne v}]/[\text{Ne III}] \lambda$ 3869  $\lesssim 0.28$ . Both of these limits are close to the SF/AGN boundary or in the ‘‘composite’’ range and compatible with

photoionization by stars (Shirazi & Brinchmann 2012; Cleri et al. 2023). Classical optical diagnostics (the so-called BPT diagrams) and rest-UV emission line diagnostics are not available for GN-z9p4, since the required lines are not detected or not covered by the NIRSpec observations. In fact, all observed emission line ratios are typical of compact, metal-poor star-forming galaxies, as can be seen by a simple comparison with Schaerer et al. (2022) showing SDSS measurements from Izotov et al. (2021). Finally, the spectrum of source shows no broad lines, although the resolution is low. More precisely, we measure a  $\text{FWHM}(\text{H}\beta) = 434 \pm 65$  km/s which is basically unresolved, and we do not detect any significant broad component in H $\beta$ , [O III]  $\lambda\lambda$ 4959,5007, or other lines. This excludes a substantial contribution of a type 1 AGN ( $\text{FWHM} > 1000$  km/s); e.g., if a type-1 AGN contributes  $> 50\%$  of the H $\beta$  flux, we would expect  $\text{FWHM}(\text{H}\beta) > 700$  km/s. In short, from the available data we find no indication for AGN, and the emission lines are compatible with those of metal-poor star-forming galaxies, although better spectra may be needed to establish this more firmly.

**Table 2.** ISM properties, ionic and total heavy element abundances (derived assuming no extinction) and other properties of GN-z9p4

Property	Quantity
$T_e(\text{O III})$ [K]	$23018 \pm 3727$
$T_e(\text{O II})$ [K]	$14685 \pm 1328$
$12 + \log(\text{O}^+/\text{H}^+)$	$6.30 \pm 0.22$
$12 + \log(\text{O}^{2+}/\text{H}^+)$	$7.36 \pm 0.15$
$12 + \log(\text{O}/\text{H})$	$7.37 \pm 0.15$
$\log(\text{N}^{3+}/\text{H})$	$-5.22 \pm 0.38$
$\log(\text{N}^{3+}/\text{O})$	$-0.59 \pm 0.24$
$\log((\text{C}^{2+} + \text{C}^{3+})/\text{O})$	$< -1.18$
$\text{ICF}(\text{Ne}^{2+}/\text{O}^{2+})$	1.04
$\log(\text{Ne}/\text{O})$	$-0.75 \pm 0.08$
$r_{\text{eff}}(\text{F182M and F210M})$	$118 \pm 16$ pc
$r_{\text{eff}}(\text{F356W and F444W})$	$< 190$ pc
$M_{1500}$	$-21.0$
$\log(M_*)$	$8.7 \pm 0.2 M_{\odot}$
SFR	$64 \pm 14 M_{\odot} \text{ yr}^{-1}$
sSFR	$120 \pm 40 \text{ Gyr}^{-1}$
E(B-V)	$0.1 \pm 0.05$

#### 3.2. Ionic and total metal abundances

With a  $4.3\sigma$  detection of the auroral [O III] $\lambda$ 4363 line, it is possible to determine accurate abundances of the ISM in GN-z9p4, using the direct method. The electron temperature  $T_e(\text{O III})$  is used to obtain abundances of ions  $\text{O}^{2+}$ ,  $\text{N}^{3+}$ ,  $\text{Ne}^{2+}$ , and upper limits for  $\text{C}^{3+}$  and  $\text{C}^{2+}$ ; the temperature in the low-ionization region,  $T_e(\text{O II})$ , to derive the ionic abundance of  $\text{O}^+$ . In the absence of direct constraints on the electron density, we adopt  $n_e = 100 \text{ cm}^{-3}$  (low density regime) and for densities  $n_e \lesssim 10^5 \text{ cm}^{-3}$  our results are essentially unchanged (abundance ratios approximately within the quoted uncertainties). Ionic abundances are derived following Izotov et al. (2006) for the optical lines. For  $\text{Ne}^{2+}$  we use the ionization correction factor (ICF) following Izotov et al. (2006). The  $\text{N}^{3+}/\text{H}^+$  abundance is determined

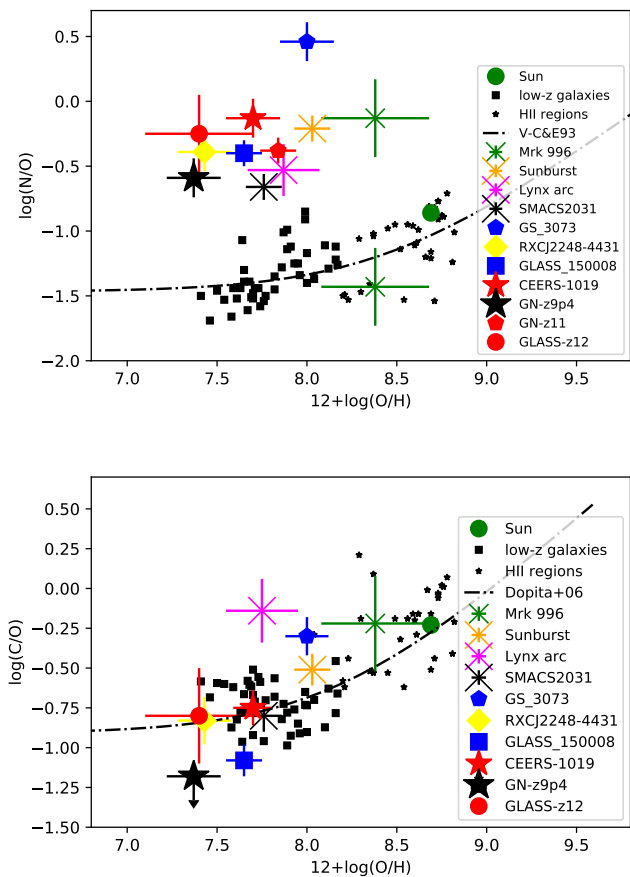


**Fig. 2.** Observed chemical abundances of all known N-emitters including GN-z9p4. *Top:* N/O versus O/H, *bottom:* C/O versus O/H. GN-z9p4 is shown by a black star. The N-emitters are sorted by increasing redshift in the legend. Only one measurement (for the densest region) is shown for GS\_3073. For Mrk 996, two N/O are available, probing regions of low and high density (James et al. 2009). Low- $z$  star-forming galaxies and HII regions from the compilation of Izotov et al. (2023) are shown by small black symbols. The dash-dotted line shows the average trend observed in low- $z$  star-forming galaxies, as parametrized by Vila-Costas & Edmunds (1993) for N/O and C/O by Dopita et al. (2006) respectively.

from the N IV] $\lambda$ 4481/H $\beta$  ratio, and upper limits on the Carbon abundance from the C III] $\lambda$ 4267 and C IV] $\lambda$ 4267 intensities with respect to H $\beta$ , following Villar-Martín et al. (2004). The results are listed in Table 2 (assuming no extinction), and the CNO abundances are shown and compared to other objects in Fig. 2. Adopting the median extinction from SED fits does not alter O/H, but would imply an increase of N/O (the C/O limit) by a factor  $\sim 2$  (1.6).

We derive a total oxygen abundance of  $12+\log(\text{O}/\text{H}) = 7.37 \pm 0.15$ , approximately 5% solar (assuming a solar value of  $12+\log(\text{O}/\text{H})=8.69$ ; Asplund et al. 2009), which is dominated by the ionic abundance of  $\text{O}^{2+}/\text{H}^+$ . This makes GN-z9p4 the N-emitter with the lowest-metallicity determined from the direct method. The ionic abundance of  $\text{N}^{3+}$  indicates a very high N/O abundance ( $\log(\text{N}^{3+}/\text{O}) = -0.59 \pm 0.24$ ), approximately 1.9 times solar, for the low metallicity (cf. Asplund et al. 2021). From the non-detection of the Carbon lines we derive an upper limit of  $\log(\text{C}/\text{O}) < -1.18$ , sub-solar but fairly representative of C/O in other metal-

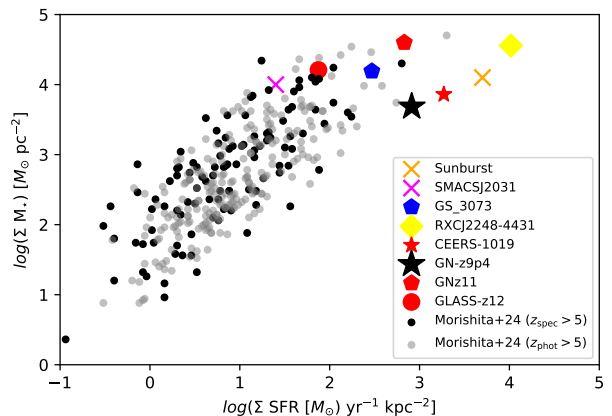


**Fig. 3.** Observed mass and SFR surface densities of the known N-emitters including GN-z9p4 compared to the sample of 341 star-forming galaxies at  $5 < z < 14$  observed with JWST, analysed by Morishita et al. (2024). Among those, objects with spectroscopic and photometric redshifts are distinguished.

poor galaxies (Izotov et al. 2023). Finally, the Neon abundance ratio  $\log(\text{Ne}/\text{O}) = -0.75 \pm 0.08$  is compatible with the average value of  $\log(\text{Ne}/\text{O}) = -0.80 \pm 0.01$  determined for normal star-forming galaxies by Guseva et al. (2011) at the same metallicity.

Together with the strongly lensed star-forming clump RXCJ2248-4431 at  $z = 6.1$  where the metallicity has also been measured from the direct method (Topping et al. 2024), and with GHZ2 at  $z = 12.34$  (Castellano et al. 2024; Zavala et al. 2024) where the metallicity is inferred only indirectly, GN-z9p4 is among the lowest-metallicity N-emitters known so far.

Taken together, the derived abundances of GN-z9p4 show that this object has a “metallicity” (O/H) of approximately 5% solar, an very high N/O abundance, and a fairly normal C/O abundance, when compared to galaxies of similar metallicity (see Fig. 2). These unusual abundance patterns are shared with the other known N-emitters, which are also shown in color in this figure. The origin of the observed N-enrichment and other abundance ratios has been discussed earlier (see Introduction), and is subject of intense research. It is beyond the scope of this Letter.

For very high electron densities,  $n_e > 10^5 \text{ cm}^{-3}$ , the inferred electron temperature would be lower, leading to a higher O/H and even more extreme (higher) N/O and C/O ratios, further highlighting the peculiarity of this source.

### 3.3. Compactness, mass and SFR surface density of GN-z9p4

We investigate the morphology of GN-z9p4 using the PySersic code (Pasha & Miller 2023) to fit its light distribution in the four NIRCcam filters. This process uses a 2D Gaussian function convolved to the instrumental point spread function (PSF) obtained from nearby bright stars in the NIRCcam field-of-view. The fitting process is performed on  $\simeq 2'' \times 2''$  background-subtracted cutouts centered on GN-z9p4. To check whether the source is spatially resolved we compare the residuals obtained from the best-fit model using a Gaussian profile to that obtained with a point source. We find that GN-z9p4 is compact, but resolved in the NIRCcam F182M and F210M bands, for which

we obtained a consistent effective radius of  $r_{\text{eff}} = 118 \pm 16$  pc. At longer wavelengths, the best-fit models assuming Gaussian and point source profiles yield both similar residuals, suggesting that GN-z9p4 is unresolved in F356W and F444W ( $r_{\text{eff}} < 190$  pc).

To determine the main properties of the stellar content of GN-z9p4 we have used the CIGALE and Bagpipes codes of Boquien et al. (2019); Carnall et al. (2018) to fit the multi-band SED, and we have added fluxes of the main emission lines and/or the full PRISM spectrum in the fits. Redshift and metallicity are fixed and a variety of star-formation histories and attenuation laws were explored<sup>2</sup>. The overall results do not strongly depend on these assumptions, in particular since the spectrum is largely dominated by a young stellar population from the rest-UV to  $5.4 \mu\text{m}$ . For this reason the stellar mass is, however, fairly uncertain. All SED fits indicate the presence of some dust attenuation. The main derived quantities, obtained using the SMC extinction law, are summarised in Table 2.

### 3.4. N-emitters are compact and rare

As already noticed early on, N-emitters show high ISM densities ( $n_e \sim 10^{3-5} \text{ cm}^{-3}$ ), or indications for regions with different densities, including densities spanning a wide range, up to high densities (see Patr cio et al. 2016; Ji et al. 2024). No density diagnostic is available from the PRISM spectrum of GN-z9p4, but we suspect that it also contains some gas at high electron densities.

Another property shared by N-emitters is their compactness, as illustrated in Fig. 3, where we show the stellar mass and SFR surface density of these objects, compared to those of star-forming galaxies at  $5 < z < 14$  measured by Morishita et al. (2024) using JWST observations. For the N-emitters it is important to note that these quantities were not determined in a uniform fashion, since, for example, different assumptions were made for the SED fits to derive stellar masses, and most importantly the effective spatial resolution is much higher for lensed objects. Despite this, it is clear that the N-emitters are exclusively found among the sources with the highest stellar mass and SFR surface densities, which indicates that the observed strong N-enhancement is related to or found in the most compact star-forming regions or objects. If confirmed with larger statistical samples, this suggests that the source of N-enhancement or the physical processes leading to a high N/O abundance require very high mass and/or SFR surface densities. This, and the high ISM densities observed in N-emitters, could represent interesting constraints to distinguish different scenarios to explain their origin.

Interestingly, several other objects from the JWST sample analysed by Morishita et al. (2024) occupy the same area as the known N-emitters and are also covered by spectroscopic observations. We have therefore examined the available NIRSpec PRISM spectra, finding one or two possible new N-emitters, although the quality of the spectra is limited. This indicates that a selection by stellar mass and SFR surface density could be an efficient way to find new N-emitters.

<sup>2</sup> We adopt a concordance cosmology with  $\Omega_m = 0.272$ ,  $\Omega_\Lambda = 0.728$ , and  $H_0 = 70.4 \text{ km s}^{-1} \text{ Mpc}^{-1}$ . We have explored exponentially declining and delayed star-formation histories, Calzetti and SMC attenuation/extinction law.

The finding of  $\sim 2$  N-emitters among the 109 galaxies of Morishita et al. (2024) having JWST spectra, shows that these objects are rare, even at high-redshift ( $z > 5$ ). This is also clear from the fact that the Nitrogen lines in the UV (N IV]  $\lambda 1486$ , N III]  $\lambda 1750$ ) are not detected in stacked NIRSpec spectra of  $z > 5$  galaxies (Roberts-Borsani et al. 2024; Langeroodi & Hjorth 2024). These current data indicate that approximately 7 out of 500 ( $\sim 1-2\%$ ) galaxies spectroscopically covered by JWST are N-emitters. This simple estimate should, however, be taken with a grain of salt, since no systematic search has yet (to the best of our knowledge) been undertaken for these sources, the target selection function is not well known, and the depth and signal-to-noise of the various observations vary strongly. Proper statistical studies of the occurrence of the N-emitters remain therefore to be done.

## 4. Conclusions

Examining JWST/NIRSpec PRISM observations we have identified a compact star-forming galaxy at  $z = 9.436$  in the GOODS-North field which shows numerous strong UV-optical emission lines and a single UV line, N IV]  $\lambda 1486$ , which qualifies this object as a new N-emitter. This brings the total number of these rare and enigmatic objects to 11.

From the emission lines, including the auroral [O III]  $\lambda 4363$  line, we have determined the abundances of H, N, O, Ne, and an upper limit on C, finding  $12 + \log(\text{O}/\text{H}) = 7.37 \pm 0.15$ ,  $\text{N}/\text{O} = -0.59 \pm 0.24$ ,  $\text{Ne}/\text{O} = -0.75 \pm 0.08$ , and  $\text{C}/\text{O} < -1.18$ . These properties make GN-z9p4 the third highest-redshift (after GLASS-z12 and GN-z11) and one of the most metal-poor N-emitters (with RXCJ2248 and possibly GLASS-z12) known so far.

With a super-solar N/O abundance ratio and a fairly normal C/O for low-metallicity (O/H), the observed ISM abundances of GN-z9p4 are found to be similar to most of the previously identified N-emitters, whose origin is debated. Comparing the stellar mass and SFR surface densities of the known N-emitters with those of star-forming galaxies, we have shown that N-emitters are exclusively found at the high-end tail of the distribution (typically with  $\log(\Sigma_{M_*}) \gtrsim 3.5 \text{ M}_\odot \text{ pc}^{-2}$  and  $\log(\Sigma_{\text{SFR}}) \gtrsim 2 \text{ M}_\odot \text{ yr}^{-1} \text{ kpc}^{-2}$ ), indicating that this phenomenon probably requires peculiar conditions (e.g. high ISM densities and compact regions), physical processes or ‘‘exotic’’ sources of nucleosynthesis.

Finally, we estimate that approximately  $\sim 1 - 2 \%$  of the galaxies currently observed with JWST at  $z \gtrsim 5$  are N-emitters, quantifying that these are rare objects. We also speculate that this phenomenon could be more frequent at higher redshift.

## References

- Asplund, M., Amarsi, A. M., & Grevesse, N. 2021, *A&A*, 653, A141
- Asplund, M., Grevesse, N., Sauval, A. J., & Scott, P. 2009, *ARA&A*, 47, 481
- Bekki, K. & Tsujimoto, T. 2023, *MNRAS*, 526, L26
- Boquien, M., Burgarella, D., Roehlly, Y., et al. 2019, *A&A*, 622, A103
- Bunker, A. J., Saxena, A., Cameron, A. J., et al. 2023, *A&A*, 677, A88
- Cameron, A. J., Katz, H., Rey, M. P., & Saxena, A. 2023, *MNRAS*, 523, 3516
- Carnall, A. C., McLure, R. J., Dunlop, J. S., & Dav , R. 2018, *MNRAS*, 480, 4379

- Castellano, M., Napolitano, L., Fontana, A., et al. 2024, arXiv e-prints, arXiv:2403.10238
- Charbonnel, C., Schaerer, D., Prantzos, N., et al. 2023, A&A, 673, L7
- Cleri, N. J., Olivier, G. M., Hutchison, T. A., et al. 2023, ApJ, 953, 10
- D'Antona, F., Vesperini, E., Calura, F., et al. 2023, A&A, 680, L19
- Dopita, M. A., Fischera, J., Sutherland, R. S., et al. 2006, ApJS, 167, 177
- Eisenstein, D. J., Willott, C., Alberts, S., et al. 2023, arXiv e-prints, arXiv:2306.02465
- Guseva, N. G., Izotov, Y. I., Stasińska, G., et al. 2011, A&A, 529, A149
- Heintz, K. E., Brammer, G. B., Watson, D., et al. 2024, arXiv e-prints, arXiv:2404.02211
- Isobe, Y., Ouchi, M., Tominaga, N., et al. 2023, ApJ, 959, 100
- Izotov, Y. I., Guseva, N. G., Fricke, K. J., et al. 2021, A&A, 646, A138
- Izotov, Y. I., Schaerer, D., Worseck, G., et al. 2023, MNRAS, 522, 1228
- Izotov, Y. I., Stasińska, G., Meynet, G., Guseva, N. G., & Thuan, T. X. 2006, A&A, 448, 955
- James, B. L., Tsamis, Y. G., Barlow, M. J., et al. 2009, MNRAS, 398, 2
- Ji, X., Übler, H., Maiolino, R., et al. 2024, arXiv e-prints, arXiv:2404.04148
- Kobayashi, C. & Ferrara, A. 2024, ApJL, 962, L6
- Langeroodi, D. & Hjorth, J. 2024, arXiv e-prints, arXiv:2404.13045
- Maiolino, R., Scholtz, J., Witstok, J., et al. 2024, Nature, 627, 59
- Marques-Chaves, R., Schaerer, D., Kuruvanthodi, A., et al. 2024, A&A, 681, A30
- Morishita, T., Stiavelli, M., Chary, R.-R., et al. 2024, ApJ, 963, 9
- Nagele, C. & Umeda, H. 2023, ApJL, 949, L16
- Nandal, D., Regan, J. A., Woods, T. E., et al. 2024, arXiv e-prints, arXiv:2402.03428
- Oesch, P. A., Bouwens, R. J., Illingworth, G. D., et al. 2014, ApJ, 786, 108
- Pascale, M., Dai, L., McKee, C. F., & Tsang, B. T. H. 2023, arXiv e-prints, arXiv:2301.10790
- Pasha, I. & Miller, T. B. 2023, The Journal of Open Source Software, 8, 5703
- Patrício, V., Richard, J., Verhamme, A., et al. 2016, MNRAS, 456, 4191
- Roberts-Borsani, G., Treu, T., Shapley, A., et al. 2024, arXiv e-prints, arXiv:2403.07103
- Schaerer, D., Marques-Chaves, R., Barrufet, L., et al. 2022, A&A, 665, L4
- Senchyna, P., Plat, A., Stark, D. P., et al. 2024, ApJ, 966, 92
- Shirazi, M. & Brinchmann, J. 2012, MNRAS, 421, 1043
- Topping, M. W., Stark, D. P., Senchyna, P., et al. 2024, MNRAS, 529, 3301
- Vila-Costas, M. B. & Edmunds, M. G. 1993, MNRAS, 265, 199
- Villar-Martín, M., Cerviño, M., & González Delgado, R. M. 2004, MNRAS, 355, 1132
- Vink, J. S. 2023, A&A, 679, L9
- Watanabe, K., Ouchi, M., Nakajima, K., et al. 2024, ApJ, 962, 50
- Weibel, A., Oesch, P. A., Barrufet, L., et al. 2024, arXiv e-prints, arXiv:2403.08872
- Zavala, J. A., Castellano, M., Akins, H. B., et al. 2024, arXiv e-prints, arXiv:2403.10491